1 **Classification: Biological Sciences; Cell Biology**

2 *Drosophila* Sex Peptide Controls the Assembly of Lipid Microcarriers in 3 Seminal Fluid

4

5 S. Mark Wainwright[a], Cláudia C. Mendes[a], Aashika Sekar[a], Benjamin Kroeger[a], Josephine
6 E.E.U. Hellberg[a], Shih-Jung Fan[a], Abigail Pavey[a], Pauline Marie[a], Aaron Leiblich[a], Carina
7 Gandy[a], Laura Corrigan[a], Rachel Patel[a], Stuart Wigby[b,c], John F. Morris[a], Deborah C.I.
8 Goberdhan[a], Clive Wilson[a]

9 [a] Department of Physiology, Anatomy and Genetics, University of Oxford, South Parks Road,
10 Oxford, OX1 3QX, UK

11 [b] Department of Zoology, University of Oxford, Oxford, OX1 3PS, UK

12 [c] Applied Zoology, Faculty Biology, Technische Universität Dresden, Dresden, Germany

13

14 Corresponding Author: Clive Wilson

15 Tel: 44 1865 282662

16 e-mail: clive.wilson@dpag.ox.acuk

17

18 Keywords: Reproduction, secretion, seminal proteins, triacylglycerides, Sex Peptide,
19 *Drosophila*

Abstract

Seminal fluid plays an essential role in promoting male reproductive success and modulating female physiology and behaviour. In the fruit fly, *Drosophila melanogaster*, Sex Peptide (SP) is the best-characterised protein mediator of these effects. It is secreted from the paired male accessory glands (AGs), which, like the mammalian prostate and seminal vesicles, generate most of the seminal fluid contents. After mating, SP binds to spermatozoa and is retained in the female sperm storage organs. It is gradually released by proteolytic cleavage and induces several long-term post-mating responses including ovulation, elevated feeding and reduced receptivity to remating, primarily signalling through the SP receptor (SPR). Here, we demonstrate a previously unsuspected SPR-independent function for SP. We show that, in the AG lumen, SP and secreted proteins with membrane-binding anchors are carried on abundant, large neutral lipid-containing microcarriers, also found in other SP-expressing *Drosophila* species. These microcarriers are transferred to females during mating, where they rapidly disassemble. Remarkably, SP is a key assembly factor for microcarriers and is also required for the female disassembly process to occur normally. Males expressing non-functional SP mutant proteins that affect SP's binding to and release from sperm in females also do not produce normal microcarriers, suggesting that this male-specific defect contributes to the resulting widespread defects in ejaculate function. Our data therefore reveal a novel role for SP in formation of seminal macromolecular assemblies, which may explain the presence of SP in *Drosophila* species, which lack the signalling functions seen in *D. melanogaster*.

Significance Statement

Seminal fluid plays a critical role in reprogramming female physiology and behaviour to promote male reproductive success. We show in the fruit fly that specific seminal proteins, including the archetypal 'female-reprogramming' molecule Sex Peptide, are stored in male seminal secretions in association with large neutral lipid-containing microcarriers, which rapidly disperse in females. Related structures are also observed in other Sex Peptide-expressing *Drosophila* species. Males lacking Sex Peptide have structurally defective microcarriers, leading to abnormal cargo loading and transfer to females. Our data reveal that this key signalling molecule in *Drosophila* seminal fluid is also a microcarrier assembly factor that controls transfer of other seminal factors, and that this may be a more evolutionarily ancient role of this protein.

Introduction

In addition to spermatozoa, semen contains a complex cocktail of macromolecules and nutrients secreted by the accessory glands of the male reproductive tract. In humans, seminal plasma nutrients include fructose from the seminal vesicles and triglycerides, both major energy sources for sperm in the female (1). In addition, enzymes, such as proteases and lipases, non-enzymatic binding proteins, like lectins and cysteine-rich secretory proteins (CRISPs), and a wide range of hormones and signalling molecules are major components, many of them generated in the prostate gland (2, 3). These molecules may be stored for days in the gland following cellular secretion, prior to being delivered to females during mating, when mixing of seminal plasma components can trigger enzyme and signal activation (4). However, the mechanisms that underpin these storage and activation events are generally not well understood.

The paired *Drosophila melanogaster* male accessory glands (AGs) share functional similarities with both the prostate and seminal vesicles in humans (5). The monolayer epithelium of these glands is formed from two secretory cell types, about 1000 main cells and 40 secondary cells at the distal tip (6)(Fig. 1A, A'). This glandular epithelial tube surrounds a large lumen. The AG secretome and its functions have been extensively characterised and multiple bioactive Accessory gland proteins (Acps) identified (7, 8). Several of these induce behavioural and physiological changes in mated females. The archetypal Acp is Sex Peptide (or Acp70Aa), a 36 amino acid protein, which is synthesised by main cells (9, 10). On transfer to females following mating, SP effects a comprehensive reprogramming of female physiology and behaviour. It promotes long-term increases in egg-laying, reduces female receptivity to remating (11, 12) and affects sperm release (13), diet

(14), feeding behaviour (15), water balance (16), defaecation (17), sleep (18), immunity (19), aggression (20) and memory (21).

Maintaining this complex post-mating response (PMR) requires SP association with the sperm plasma membrane after mating (12). Sperm can then be stored for several weeks in two female organs, the paired spermathecae and the seminal receptacle, with SP gradually released by proteolytic cleavage to mediate its effects (22).

Studies in which SP or SP mutant peptides are either injected or expressed ectopically in females have demonstrated that SP can induce many of the characterised female PMRs, with distinct molecular domains in SP having different functions eg., (9, 23, 24). In females, the SP receptor (SPR) is required to mediate most of these effects (25). SPR is expressed in specific neurons of the female reproductive tract that have a key role in the SP-dependent PMR (26, 27), and in other neurons in the CNS that are also able to respond to circulating SP (28, 21). In addition, SP appears to produce some SPR-independent post-mating responses in females (29, 20).

Here we report a novel SPR-independent function for SP in males, involving storage and delivery of seminal components. We show that the AG lumen is filled with many large, fusiform- and ellipsoid-shaped microcarriers containing a neutral lipid core and coated with specific proteins such as SP. Microcarriers rapidly dissipate on transfer to females after mating, providing a simple mechanism for timely release of stored seminal proteins. Surprisingly, we find that SP is essential for assembly of microcarriers in males, and that this function is required for the normal delivery of microcarrier-associated macromolecules and nutrients to the female reproductive tract during mating. Furthermore, we identify related microcarrier structures in other *Drosophila* species that express a Sex Peptide and show that

101 the size and shape of microcarriers has changed as the amino acid sequence of Sex Peptide
102 evolved in these species.

103

104 **Results**

105 **The lumen of the accessory gland is filled with large neutral lipid-containing microcarriers**

106 While analysing the lipid content of epithelial cells within the male AG, using the lipophilic
107 dye Nile Red, which stains membranes and lipid droplets, we observed that the large AG
108 lumen is filled with fluorescent fusiform structures typically 3-8 µm in length (Fig. 1B, B').
109 These structures were of variable diameter ranging from less than 0.5 µm to a maximum of
110 4.0 µm (Fig. S1I). Since these structures were found to bind specific main cell proteins (Fig.
111 2A), we call them 'microcarriers'. The neutral lipid-specific dye LipidTox Red stained
112 microcarriers highly selectively (Fig. 1C, C'), suggesting they contain large quantities of
113 triglycerides and other non-polar lipids. Microcarriers were also detected using high
114 concentrations of the acidophilic, but partially hydrophobic, LysoTracker dyes (Fig. 1D; (30)).
115 By contrast, in fixed tissue, microcarriers exclude access to antibodies raised against soluble
116 secreted AG proteins, such as angiotensin I-converting enzyme (ANCE; Fig. 1E). Microcarriers
117 are not an artefact of fixation or staining, because they are readily discernable in living
118 glands using Differential Interference Contrast (DIC) microscopy (Fig. 1F).

119 Previous studies have shown that some transmembrane proteins expressed in epithelial
120 secondary cells of the AG are secreted on exosomes (31). When transmembrane proteins
121 were expressed in main cells, they did not associate with microcarriers (Fig. 1G, S1A, A') and
122 neither did dyes like PKH26 that bind to lipid bilayers (Fig. S1B, B'). A secreted form of GFP,

123 comprised of the SP signal sequence fused to GFP (24), also failed to preferentially bind to
124 microcarriers (Fig. S1C). By contrast, GFP-GPI, a GFP fusion protein carrying the lipid anchor
125 glycosylphosphatidylinositol, strongly labelled microcarriers when expressed in main cells
126 (Fig. 1H, H'), but not when made in secondary cells (Fig. S1D, D'; (32)), consistent with the
127 idea that main cells produce these structures. Indeed, a concentrated layer of GFP-GPI-
128 positive staining was observed at the apical surface of main cells overexpressing this
129 transgene (Fig. 1H'), reflecting the shedding of lipophilic material from these cells. In the
130 largest microcarriers, GFP-GPI, unlike LipidTox staining (Fig. 1C, C'), was surface-localised
131 (Fig. 1H, H'), suggesting that these structures have a distinct outer layer, most likely a
132 phospholipid monolayer into which the GPI anchor is inserted, surrounding the neutral lipid
133 core. Although microcarrier ultrastructure was difficult to preserve for transmission electron
134 microscopy, micrographs were consistent with these structures having a homogeneous
135 internal structure (Fig. S1E).

136

137 **Sex Peptide is a microcarrier cargo**

138 An SP-GFP C-terminal GFP fusion protein expressed in main cells under the control of *SP*
139 gene regulatory elements (33) has previously been used to assess SP transfer to females.
140 Surprisingly, we found that it strongly associates with microcarriers and concentrates at the
141 surface of the largest structures, but is present at very low levels within main cells (Fig. 2A,
142 B; SI Movie 1). When SP-GFP males were mated, fluorescently labelled microcarriers were
143 transferred to females (Fig. 2C, D). We were unable to detect microcarriers using neutral
144 lipid stains in the female reproductive tract, at least partly because of poor dye penetration.
145 However, using SP-GFP as a marker, we found that 25 min after the start of mating (ASM),

which is typically within five minutes of the end of mating, microcarriers had already started to change their morphology (Fig. 2E, E'). Although their basic fusiform shape was frequently still distinguishable, SP-GFP concentrated in microdomains on the microcarrier surface. Later, at 45 min ASM, smaller spherical SP-GFP-positive puncta were dispersed throughout the uterus and SP-GFP was observed on a subset of sperm tails (Fig. 2F, F'), while later still (60 min ASM), more of the SP-GFP (Fig. 2G, G') was associated with sperm tails. However, at 90 min ASM, only very weak, if any, GFP expression was observed on sperm in the sperm storage organs (Fig. 2H-I'), either because the most strongly labelled sperm do not migrate to these organs or because the GFP tag is lost over time. Microcarriers that are ejected from the AG, but remain in the male ejaculatory duct after mating, do not break down (Fig. 2J, J'), suggesting that microcarrier dissipation is triggered by physical or chemical signals inside the uterus.

To confirm that C-terminal tagging of SP with GFP does not affect SP's binding properties in the AG lumen and to begin to dissect out what domains in SP bind to microcarriers, we overexpressed three SP-GFP fusions in main cells under GAL4/UAS control: the N-terminal half of mature SP fused at its C-terminus to GFP (SPn-GFP), the C-terminal half of SP fused at its N-terminus to GFP (GFP-SPc), and a fusion with GFP located in the centre of the SP protein (SPn-GFP-SPc). The latter has been shown to have biological activity in females (24). Using the main cell-specific *Acp26Aa*-GAL4 driver (Fig. 1A) (11), which expresses at lower levels than GFP-tagged SP under its own promoter, all SP fusions partitioned with microcarriers (Fig. S1F-H), albeit less selectively for the N-terminal SP construct, SPn-GFP. Microcarriers therefore appear to bind to both the N- and C-terminal domains of SP. We conclude that they act as stores for SP, other seminal proteins, such as those with a GPI

anchor, and neutral lipids in males, and serve as vehicles for their transfer to females. Regulated microcarrier disassembly in females presumably assists in the timely release of lipids and seminal proteins, such as SP, after mating.

SP controls microcarrier morphology via an SPR-independent mechanism

To assess whether *SP* is involved in microcarrier assembly, we analysed AGs of males carrying the previously generated SP^0 null allele (12), either as a homozygote or in transheterozygous combination with a small *SP* deficiency, *Df(3L)Δ130* (35, 12). These transheterozygous *SP* null males have been used to characterise the full range of *SP* mutant PMR phenotypes (12-21). Unexpectedly, these mutant animals displayed dramatic defects in microcarrier morphology (Fig. 3A-D, I-J; S2A, B; S3A). Most microcarrier-like structures were highly enlarged, and either spherical or ellipsoid in shape. The enlarged microcarrier phenotype was never observed in wild type glands (Fig. 3A, C). In confocal images of the AG lumen, 10/10 $SP^0/Df(SP)$ null glands had microcarriers with a minimum width greater than 10 µm, whereas 0/10 wild type glands contained such structures (P<0.0001; Fisher's exact test). The enlarged microcarriers from the $SP^0/Df(SP)$ null glands were uniformly stained by LipidTox. They appeared like large lipid droplets under DIC (Fig. 3D). The defects were absent in SP^0 $SP^+/Df(3L)Δ130$ males, which express an *SP* genomic rescue construct that rescues the PMR phenotypes in mated females (12) (Fig. 3E); 0/10 *SP* rescue glands had microcarriers with a minimum width greater than 10 µm (P<0.0001 versus $SP^0/Df(SP)$). Automated measurement of minimum microcarrier diameter in individual images of male AGs with these different genotypes confirmed the change in size distribution in the *SP* null background (Fig. 3I). Mating $SP^0/Df(SP)$ null males multiple times with females over several

192 days to mix and eject the AG's contents, exacerbated the mutant phenotype, with some
193 microcarriers spanning the entire diameter of the AG lumen (Fig. 3F, G), suggesting that
194 microcarriers can enlarge by fusion. When seminal fluid remained in the ejaculatory duct of
195 *SP^{0}/Df(SP)* null males after mating, the duct lumen was also filled with enlarged
196 microcarriers (Fig. 3H).

197 To confirm that SP expression in main cells is required for normal microcarrier assembly, we
198 knocked down *SP* transcripts specifically in these cells, using the GAL4/UAS system (35),
199 employing the *Acp26Aa*-GAL4 driver (11). Although limited effects were observed when
200 these experiments were performed at 25°C, expression of *SP*-RNAis from three different
201 transgenic lines at 29°C, a temperature that typically enhances GAL4-induced expression
202 (36), produced consistent marked defects in microcarrier morphology (Fig. 4A-C, Fig. S2C, D,
203 Fig. S3B). Microcarriers were enlarged in all three knockdowns, though to a lesser extent
204 than in *SP^{0}/Df(SP)* null males. As observed in mated *SP^{0}/Df(SP)* null males (Fig. 3G), mating
205 greatly exacerbated the size phenotype (Fig. 4E, F).

206 In females, many of SP's activities in modulating the female PMR are mediated by the SPR
207 (25). However, *SPR* mutant males displayed completely normal microcarriers (Fig. 4G),
208 demonstrating that SP acts independently of the SPR in the male AG, presumably via direct
209 interaction with microcarriers.

210 Binding of SP to the plasma membrane of sperm in females requires a short peptide
211 sequence at the N-terminal end of the mature molecule (22). This region must be
212 proteolytically removed for SP to be released from sperm in the sperm storage organs. Two
213 mutants expressed under the control of the SP promoter, one that lacks the N-terminal
214 membrane-association domain (SP$^{\Delta 2\text{-}7}$) and the other mutated at the proteolytic cleavage

site (SP^{QQ}), have both previously been shown to fail to induce the long-term PMR in females (22). These constructs also failed to rescue the microcarrier phenotype in *SP^0/Df(SP)* null males (Fig. 4H-K; Fig S3C). For both mutants, 7/7 glands had microcarriers with a minimum width greater than 10 µm (Fig. S3C), suggesting that the N-terminal region of SP, which appears to bind microcarriers (Fig. S1F), plays an important role in microcarrier assembly, as well as sperm binding.

Microcarriers from *SP* mutant males do not disassemble normally in females after mating

A key property of microcarriers is that they are stable in the male AG, yet change their morphology within minutes, when transferred to females. We tested how this process is affected in *SP* mutants. Since the C-terminally tagged SP-GFP construct, which has previously been reported to lack normal SP activity in females (23), failed to rescue the *SP^0/Df(SP)* null microcarrier phenotype in males (Fig. 5B), we used this as an alternative to neutral lipid dyes to mark microcarriers. SP-GFP distributed evenly throughout the enlarged microcarriers in *SP^0/Df(SP)* null males (Fig. 5A, B).

Unlike in controls (Fig. 5C), microcarriers from *SP^0/Df(SP)* null males failed to rapidly dissipate in females and instead formed a homogeneously stained mass in the uterus (Fig. 5D), which did not break down during the period when SP-GFP is normally transferred to sperm tails (compare Fig. 5G, G' with Fig. 5H, H'); indeed, unlike controls, the mass extended into the anterior uterus with some sperm tails embedded within it. We conclude that normal dissipation and distribution of microcarrier cargos is disrupted in females mated

with *SP^{0}/Df(SP)* null males, and this is likely to contribute to the aberrant post-mating phenotypes observed in mated females.

SP and microcarrier structure have rapidly co-evolved in *Drosophila* species

To test whether other *Drosophilidae* might employ a similar neutral lipid-based strategy to package molecules in seminal fluid, we stained the AGs of multiple *Drosophila* species with LipidTox (Fig. 6). Species closely related to *D. melanogaster*, namely *D. simulans* and *D. sechellia* (Fig. 6A), had microcarriers with remarkably similar size and shape (Fig. 6B-D). AGs of the species, *D. yakuba*, and *D. erecta*, which are still members of the *melanogaster* group but have more divergent SP structure (24) (Fig. S4), also contained microcarriers, but these were more spherical in shape (Fig. 6E, F).

Examining more distantly related *Drosophila* species with more diverged SP proteins (Fig. S4) revealed very different microcarrier organisation. *D. pseudoobscura* and *D. persimilis*, both members of the *obscura* group, have smaller spherical microcarriers that appear to be more widely separated (Fig. 6G, H).

Two further *Drosophila* species *D. willistoni* and *D. virilis* express forms of SP with major structural differences to the *melanogaster* and *obscura* groups. These proteins not only lack a central 10 amino acid portion of the molecule, including the sequence required for proteolytic cleavage, but have also diverged considerably in other regions with the exception of the last 15 C-terminal amino acids (Fig. S4). Bright-field and DIC microscopy revealed *D. willistoni* glands have densely packed globular structures that can be stained with LipidTox, although this is most clearly observed in punctured glands (Fig. 6I-I''). The *D.*

virilis AG, whether intact or cut, showed little evidence of LipidTox-stained microcarriers (Fig. 6J) and bright-field and DIC imaging suggested a more uniform "flocculence" (Fig. 6J', J''). Finally, we examined the AGs of *D. mojavensis*, a species that lacks an SP homologue (Fig. S4). Although there were some large spherical structures in the gland lumen in DIC images, no LipidTox-positive staining was observed in these glands (Fig. 6K-K'). Therefore, our analysis suggests that the divergence of SP structure closely parallels changes in microcarrier shape, size and density.

Discussion

Seminal fluid plays an essential role in male reproductive success. In *D. melanogaster*, SP, produced from the male AG, has been highlighted as a central player in this process, acting via receptors in the female to stimulate changes that increase fecundity and prevent remating. Here we demonstrate that SP has an additional, unsuspected role in males in the assembly of neutral lipid-containing microcarriers in the AG lumen (summarised in Fig. 5I). These microcarriers store SP, other proteins with lipid anchors or potentially hydrophobic domains, and neutral lipids, so that they can be delivered to females during mating, and dispersed rapidly in the female reproductive tract. Our analysis of microcarriers in other *Drosophila* species reveals that SP's microcarrier assembly function may exist in species in which SP has more limited roles in modulating the PMR, suggesting that this function might have been critical in the evolution of this molecule.

Lipid microcarriers provide a store, delivery vehicle and dispersal machinery for a subset of seminal proteins.

Seminal proteins are produced throughout adult life, but these proteins are only transferred to females sporadically. Some of these proteins are then rapidly activated via mechanisms that are thought to include proteolytic cleavage and pH changes in the female reproductive tract (discussed in (5)). Our data suggest that microcarriers could contribute to this activation process. They are repositories for main cell-derived seminal proteins, which presumably partition from the aqueous phase of the AG's secretions, either because of their lipophilicity or because they have binding partners on the microcarrier surface. In the male, molecules like SP bind specifically to microcarriers and not to AG epithelial cells, strongly suggesting that these surfaces are structurally distinct. Subsequent microcarrier dissipation in the female reproductive tract provides a mechanism for dispersing proteins like SP, so they can associate with receptors and cell membranes following mating.

Although both staining of normal microcarriers with lipophilic dyes and the homogeneous internal structure of large defective *SP^{0}/Df(SP)* null 'microcarriers' observed with DIC strongly suggest that neutral lipids are a major component of these structures, their precise composition remains unclear. In addition, their non-spherical shape in wild type males suggests that architectural proteins are highly likely to be involved in establishing their final structure, a proposal supported by the *SP* mutant phenotype. It will now be important to identify these other structural constituents and to establish whether any of these, unlike SP, play evolutionarily conserved roles in seminal fluid production outside the *Drosophilidae* family.

Analysis of transcriptomics data from adult *Drosophila* organs reveals high level expression in the AG of multiple lipases that are predicted to be secreted (eg., CG5162, CG11598, CG11600, CG11608, CG13034, CG18258, CG18284, CG31872, CG34447; (37), (38), with all having been detected in proteomics analyses of seminal fluid (39, 8). These include proteins sharing homology with triacylglycerol lipases (eg., CG5162, CG13034, CG18258, CG34447). These lipases provide a potential mechanism to break down neutral lipid transferred in microcarriers to females, so the products can be used as fuel. Mammalian seminal fluid also contains lipases (40, 41, 42) and triacylglycerides (43, 44), suggesting that the latter may be required, perhaps as a male-derived nutrient source, in the reproductive system of all higher organisms.

Our identification of extracellular neutral lipid microcarriers as accessible stores of specific seminal proteins is reminiscent of the role of intracellular lipid droplets in storage of cytoplasmic and nuclear proteins (45, 46). Lipid droplets are able to dock with specific intracellular organelles to mediate their functions and deliver their cargos. It will be interesting to investigate whether the remnants of microcarriers, such as the microdomains observed with SP-GFP, are in any way targeted to specific cells or structures after transfer to females, as these storage vehicles break down.

It has previously been reported in *Drosophila* that males can adaptively modulate the relative balance of seminal proteins, including SP, in the ejaculate, depending on female mating status and the presence of rival males (47, 48). Loading of selected proteins on to microcarriers might provide a simple mechanism to control such rapid changes, if the transfer of these large structures can be differentially regulated compared to soluble

proteins, for example by controlling the opening of the sphincters through which seminal fluid passes from the AGs to the ejaculatory duct.

Regulation of microcarrier morphology by SP and microcarrier/SP co-evolution in *Drosophila.*

Our study reveals a previously unsuspected male-specific, SPR-independent role for SP in regulating microcarrier shape and size. *SP* mutants in *D. melanogaster* still have neutral lipid-containing structures, but they appear to aggregate and fuse, particularly after mating, to generate large lipid droplet-like structures that no longer retain molecules like SP at their surface. To date, we have not been able to separate the different activities of SP in males and females through expression of different mutants or altered SP levels, making it difficult to fully gauge the importance of the male-specific microcarrier function. However, the observation that *SP* mutants, which were known to affect binding of SP to the surface of sperm or its subsequent release, also fail to rescue the microcarrier defect in *SP* null males, suggests that the interpretation of the phenotypes associated with these mutants requires some re-evaluation.

Tsuda et al. (24) have suggested that SP is likely to have roles in addition to its effects mediated via SPR signalling in the female reproductive tract, which include induction of a female sexual refractory period. This is because some SP-expressing species like *D. pseudoobscura* and *D. persimilis* do not appear to express SPR in this location and additionally show much female less post-mating refractoriness relative to other SP-producing species (49). Our data (Fig. 6) suggest that microcarrier assembly may be this

345 additional function with the shape of microcarriers rapidly co-evolving with SP, and an
346 absence of microcarriers in species with a highly divergent (*D. virilis*) or no (*D. mojavensis*)
347 SP homologue. It will be interesting to investigate whether other proteins with fundamental
348 roles in packaging and storing seminal fluid components have also evolved signalling roles in
349 some species.

350 An important conclusion from our study is that the normal transfer of several different
351 seminal proteins is likely to be interdependent. Elegant studies by the Wolfner lab have
352 identified several long-term response (LTR) network genes expressed in the AG that are
353 required either in the male or female for SP to be retained in the sperm storage organs (50,
354 51, 52). It will be important to investigate whether any of these genes is involved in loading
355 or unloading SP from microcarriers, or indeed, whether they play a role in microcarrier
356 assembly. Furthermore, determining whether other Acps or main cell-expressed GPI-
357 anchored proteins are microcarrier cargos should allow the functions of these structures to
358 be assessed more extensively and may suggest molecular tools that could be used to screen
359 for similar processes in higher organisms.

360

361 **Materials and Methods**

362 ***Drosophila* Stocks and Genetics**

363 Fly stocks were obtained from the following sources: the Bloomington *Drosophila* Stock
364 Center provided *UAS-GFP.nls* (53)3, *UAS-mCD8-GFP* (54), *tub-GAL80^{ts}* (55), *UAS-SP-RNAi#2*
365 TRiP.JF02022 (56), *UAS-mCD8-ChRFP*; the Vienna *Drosophila* Resource Center provided *UAS-*
366 *SP-RNAi#3* (v109175); the Kyoto DGRC Stock Center provided *spi-GAL4* (57); S. Goodwin

provided *dsx-GAL4* (58), *Acp26Aa-GAL4* (11), *SP-GFP* (33); T. Aigaki provided *UAS- SPn-GFP-SPc, UAS-SPn-GFP, UAS-GFP-SPc, UAS-sGFP* (24); M. Wolfner provided SP^{QQ}, $SP^{\Delta 2\text{-}7}$ (22), *Df(SPR)* (25); S. Eaton provided *UAS-GFP-GPI* (59); T. Chapman provided SP^{0}, SP^{0} SP^{+} (12), *Df(3L)Δ130* (34), *UAS-SP-RNAi-IR2* (RNAi#1; (11)); L. Partridge provided w^{1118}. A. McGregor provided *D. simulans, D. sechellia, D. yakuba, D. pseudoobscura, D. virilis* and the Gulbenkian Institute provided *D. erecta, D. persimilis, D. mojavensis.*

Fly husbandry

Flies were maintained on standard cornmeal agar food (12.5 g agar, 75 g cornmeal, 93 g glucose, 31.5 g inactivated yeast, 8.6 g potassium sodium tartrate, 0.7 g calcium, and 2.5 g Nipagen [dissolved in 12 ml ethanol] per litre) at 25°C on a 12:12-h light:dark cycle. Males for *SP* knockdown or those with *tub-GAL80*^{ts} were shifted to 29°C on eclosion to activate UAS-transgenes.

Staining and immunostaining of fly reproductive tracts

Unless otherwise stated, 3-4-day-old virgin males were used for AG dissection and for mating experiments. 4-7-day-old w^{1118} virgin females were used for mating experiments. For fixed tissues, reproductive tracts were dissected in 4% paraformaldehyde (Sigma-Aldrich) in PBS (Gibco). AGs with the ejaculatory duct attached were fixed for 20 min and rinsed at least four times in PBS prior to further treatments. For females the abdomen was carefully opened up and fixative allowed to permeate internally for 20 min prior to removal of the uterus with seminal receptacle, spermathecae and common oviduct attached. Reproductive tracts were washed four times with PBS.

Fixed accessory glands were stained at room temperature in the following solutions and then washed four times in PBS: 1:50 dilution in PBS of a 10 mg/ml solution of Nile red (Sigma-Aldrich) dissolved in acetone and incubated for 30 min; 1:100 dilution in PBS of LysoTracker Deep Red (Life Technologies) for 1 h; 1:50 dilution in PBS of LipidTox (Invitrogen) for 1 h; 1:40 dilution in diluent C of a 1mM stock of PKH26 red fluorescent cell marker (Sigma-Aldrich) for 30 min; 1:1000 dilution in PBS of a 10 mg/ml stock of Hoechst 33342 (Invitrogen) for 5 min.

For live imaging, accessory glands were dissected in ice-cold PBS. Live glands requiring staining were treated for 5 min in a 1:100 dilution of LysoTracker Red DND-99 (Life Technologies) in ice-cold PBS.

For ANCE antibody staining, fixed accessory glands were permeabilised for 6 x 10 min in PBST (1 X PBS, 0.3% Triton X-100 [Sigma-Aldrich]), blocked for 30 min in PBSTG (PBST, 10% goat serum [Sigma-Aldrich]) and incubated overnight at 4°C in rabbit anti-ANCE primary antibody (60) diluted 1:2000 in PBSTG. Glands were then washed for 6 x 10 min in PBST before incubation in a 1:400 dilution of Cy-5-conjugated donkey anti-rabbit secondary antibody (Jackson Laboratories) for 2 h at room temperature. Glands were further washed in PBST for 6 x 10 min prior to mounting.

Glands stained with Hoechst were mounted in PBS; all other fixed reproductive tracts were mounted in Vectashield with DAPI (Vector Laboratories). Glands for live imaging were mounted in a small drop of ice-cold PBS surrounded by 10S Voltalef (VWR) halocarbon oil (61).

Electron microscopy

3-day-old w^{1118} male reproductive tracts were dissected and incubated overnight in 2.5% glutaraldehyde and 4% formaldehyde in PBS (pH 7.2). Glands were then washed with PBS, refixed in 1% osmium tetroxide (Agar Scientific) for 20 minutes, washed 3 times in distilled water and dehydrated through a graded alcohol series and incubated in ethanol and Spurr's epoxy resin (1:1) (Agar Scientific). Glands were embedded in 100% Spurr's epoxy resin between two sheets of polythene and polymerised overnight at 60°C. Ultrathin sections were prepared with a Reichert Ultracut R Ultramicrotome (Leica Biosystems) and mounted on formvar-coated slot grids (Agar Scientific). Sections were stained with 2% uranyl acetate and lead citrate (Agar Scientific), and imaged using a JEOL 1010 electron microscope (80kV).

Imaging

Images of fixed reproductive tracts were acquired either on a Zeiss LSM 510 Meta [Axioplan2] or a LSM 880 laser scanning confocal microscope equipped with Zeiss 10x NA 0.45, 20x NA 0.8, 40x NA 1.3 and 63x NA 1.4 objectives. Live scanning confocal imaging was performed on a Zeiss LSM 710 microscope using a 63x NA 1.4 objective. Live DIC images were acquired on a DeltaVision Elite wide-field fluorescence deconvolution microscope (GE Healthcare Life Sciences) equipped with a 100x, NA 1.4 UPlanSApo oil objective (Olympus).

Automated analysis of microcarrier size

Images were opened with Fiji software. Microcarrier image analysis was performed using the open-access CellProfiler Software version 2.2.0. A workflow for segmenting all the microcarriers and measuring the minimum feret diameter of each microcarrier was developed by adding pre-programmed algorithmic modules in a pipeline. Histograms based

on microcarrier minimum width and microcarrier area in different minimum width ranges were plotted using GraphPad Prism-8 software.

Changes in microcarrier size were further assessed by recording the presence or absence of microcarriers with a minimum width greater than 10 µm for 7-10 glands in a representative 100 μm^2 field of view of the lumen midway along the length of the gland. *P*-values were calculated using Fisher's exact test.

All materials, tools and datasets generated in this study are presented in the paper or will be made available upon request.

ACKNOWLEDGEMENTS

We thank Suzanne Eaton, Mariana Wolfner, Toshiro Aigaki, Tracey Chapman, Stephen Goodwin, Elwyn Isaac, Nuno Soares and Alistair McGregor for stocks and reagents; we are grateful to the Bloomington *Drosophila* Stock Center, the Vienna *Drosophila* Resource Center and the Kyoto DGRC Stock Centre for flies. We thank the Micron Advanced Bioimaging Unit (supported by Wellcome Strategic Awards 091911/B/10/Z and 107457/Z/15/Z) for their support & assistance in this work. We acknowledge the support of the Biotechnology and Biological Sciences Research Council (BB/K017462/1, BB/L007096/1, BB/N016300/1, BB/R004862/1 and a Fellowship to SW, BB/K014544/1), Cancer Research UK (C19591/A19076, C602/A18974), the Cancer Research UK Oxford Centre Development Fund (C38302/A12278), and the Wellcome Trust (Strategic Awards #091911, #107457 and 102347/Z/13/Z), as well as the MRC for studentship funding.

References

1. D. Montagnon, B. Valtat, F. Vignon, M. H. Koll-Back, Secretory proteins of human seminal vesicles and their relationship to lipids and sugars. *Andrologia* **22**, Suppl. 1, 193-205 (1990).

2. T.L. Veveris-Lowe, S. J. Kruger, T. Walsh, R. A. Gardiner, J. A. Clements, Seminal fluid characterization for male fertility and prostate cancer: kallikrein-related serine proteases and whole proteome approaches. *Semin. Thromb. Hemost.* **33,** 87-99 (2007).

3. J. Vitku, L. Kolatorova, R. Hampl, Occurrence and reproductive roles of hormones in seminal plasma. *Basic Clin. Androl.* **27,** 19 (2017).

4. G. Pampalakis, G. Sotiropoulou, Tissue kallikrein proteolytic cascade pathways in normal physiology and cancer. *Biochim. Biophys. Acta* **1776**, 22-31 (2007).

5. C. Wilson, A. Leiblich, D. C. Goberdhan, F. Hamdy, The *Drosophila* accessory gland as a model for prostate cancer and other pathologies. *Curr. Topics Dev. Biol.* **121,** 339-375 (2017).

6. A. Bairati, Structure and ultrastructure of the male reproductive system in *Drosophila melanogaster*: the genital duct and accessory glands. *Monitore Zool. Ital.* **2,** 105-182 (1968).

7. L. K. Sirot *et al*., Molecular social interactions: *Drosophila melanogaster* seminal fluid proteins as a case study. *Adv. Genet.* **68,** 23-56 (2009).

8. I. Sepil *et al*., Quantitative proteomics identification of seminal fluid proteins in male *Drosophila melanogaster. Mol. Cell Proteomics* **18,** S46-58 (2019).

9. P. S. Chen *et al*., A male accessory gland peptide that regulates reproductive behavior of female *D. melanogaster*. *Cell* **54,** 291-298 (1988).

475 10. E. Kubli, Sex-peptides: seminal peptides of the *Drosophila* male. *Cell. Mol. Life Sci.* **60,**
476 1689-1704 (2003).

477 11. T. Chapman *et al*., The sex peptide of *Drosophila melanogaster*: Female post-mating
478 responses analyzed by using RNA interference. *Proc. Natl. Acad. Sci. USA* **100,** 9923-9928
479 (2003).

480 12. H. Liu, E. Kubli, Sex-peptide is the molecular basis of the sperm effect in *Drosophila*
481 *melanogaster*. *Proc. Natl. Acad. Sci. USA* **100,** 9929-9933 (2003).

482 13. F. W. Avila, K. R. Ram, M. C. Bloch Qazi, M. F. Wolfner, Sex peptide is required for the
483 efficient release of stored sperm in mated *Drosophila* females. *Genetics* **186,** 595-600
484 (2010).

485 14. C. Ribeiro, B. J. Dickson, Sex peptide receptor and neuronal TOR/S6K signalling modulate
486 nutrient balancing in *Drosophila. Curr. Biol.* **20,** 1000-1005 (2010).

487 15. G. B. Carvalho, P. Kapahi, D. J. Anderson, S. Benzer, Allocrine modulation of feeding
488 behavior by the sex peptide of *Drosophila*. *Curr. Biol.* **16**, 692-696 (2006).

489 16. P. Cognigni, A. P. Bailey, I. Miguel-Aliaga, Enteric neurons and systemic signals couple
490 nutritional and reproductive status with intestinal homeostasis. *Cell Metab.* **13**, 92-104
491 (2011).

492 17. J. Apger-McGlaughon, M. F. Wolfner. Post-mating changes in excretion by mated
493 *Drosophila melanogaster* females is a long-term response that depends on sex peptide and
494 sperm. *J. Insect Physiol.* **59,** 1024-1030 (2013).

18. R. E. Isaac, C. Li, A. E. Leedale, A. D. Shirras, *Drosophila* male sex peptide inhibits siesta sleep and promotes locomotor activity in the post-mated female. *Proc. R. Soc. B* **277,** 65-70 (2010).

19. J. Peng, P. Zipperlen, E. Kubli. *Drosophila* sex-peptide stimulates female innate immune system after mating via the Toll and Imd pathways. *Curr. Biol.* **15,** 1690-1694 (2005).

20. E. Bath *et al.*, Sperm and sex peptide stimulate aggression in female *Drosophila*. *Nat. Ecol. Evol.* **1,** 0154 (2017).

21. L. Scheunemann, A. Lampin-Saint-Amaux, J. Schor,T. Preat. A sperm peptide enhances long-term memory in female *Drosophila*. *Sci. Adv.* **5,** eaax342 (2019).

22. J. Peng, S. Chen, S. Büsser, H. Liu, T. Honegger, E. Kubli, Gradual release of sperm bound sex-peptide controls female postmating behavior in *Drosophila*. *Curr. Biol.* **15**, 207-213 (2005).

23. E. V. Domanitskaya, H. Liu, S. Chen, E. Kubli, The hydroxyproline motif of male sex peptide elicits the innate immune response in *Drosophila* females. *FEBS J.* **274**, 5659-5668 (2007).

24. M. Tsuda, J. B. Peyre, T. Asano, T. Aigaki, Visualizing molecular functions and cross-species activity of sex-peptide in *Drosophila*. *Genetics* **200,** 1161-1169 (2015).

25. N. Yapici, Y. J. Kim, C. Ribeiro, B. J. Dickson A receptor that mediates the post-mating switch in *Drosophila* reproductive behaviour. *Nature* **451,** 33-37 (2008).

26. M. Häsemeyer, N. Yapici, U. Heberlein, B. J. Dickson, Sensory neurons in the *Drosophila* genital tract regulate female reproductive behavior. *Neuron* **61,** 511-518 (2009).

516 27. C. H. Yang *et al*., Control of the postmating behavioral switch in *Drosophila* females by
517 internal sensory neurons. *Neuron* **61,** 519-526 (2009).

518 28. Z. Ding, I. Haussmann, M. Ottiger, E. Kubli, Sex-peptides bind to two molecularly
519 different targets in *Drosophila melanogaster* females. *J. Neurobiol.* **55,** 372-384 (2003).

520 29. I. U. Haussmann, Y. Hemani, T. Wijesekera, B. Dauwalder, M. Soller, Multiple pathways
521 mediate the sex-peptide-regulated switch in female *Drosophila* reproductive behaviours.
522 *Proc. Biol. Sci.* **280,** 20131938 (2013).

523 30. B. Zhitomirsky, H. Farber, Y. G. Assaraf, LysoTracker and MitoTracker Red are transport
524 substrates of P-glycoprotein: implications for anticancer drug design evading multidrug
525 resistance. *J. Cell Mol. Med.* **22,** 2131-2141 (2018).

526 31. L. Corrigan *et al*., BMP-regulated exosomes from *Drosophila* male reproductive glands
527 reprogram female behavior. *J. Cell Biol.* **206,** 671-688 (2014).

528 32. S. Redhai *et al*., Regulation of dense-core granule replenishment by autocrine BMP
529 signalling in *Drosophila* secondary cells. *PLoS Genet.* **12**, e1006366 (2016).

530 33. A. Villella, J. B. Peyre, T. Aigaki, J. C. Hall, Defective transfer of seminal-fluid materials
531 during matings of semi-fertile *fruitless* mutants in *Drosophila*. *J. Comp. Physiol. A* **192,** 1253–
532 1269 (2006).

533 34. R. Nolo, L. A. Abbott, H. J. Bellen, *Drosophila Lyra* mutations are gain-of-function
534 mutations of senseless. *Genetics* **157,** 307-315 (2001).

535 35. A. H. Brand, N. Perrimon, Targeted gene expression as a means of altering cell fates and
536 generating dominant phenotypes. *Development* **118,** 401-415 (1993).

537 36. A. H. Brand, A. S. Manoukian, N. Perrimon, Ectopic expression in *Drosophila*. Methods
538 Cell Biol. **44**, 635-654 (1994).

539 37. J. L. Mueller *et al.,* Cross-species comparison of *Drosophila* male accessory gland protein
540 genes. *Genetics* **171,** 131-143 (2005).

541 38. V. R. Chintapalli, J. Wang, J. A. Dow, Using FlyAtlas to identify better *Drosophila*
542 *melanogaster* models of human disease. *Nat. Genet.* **39,** 715-720 (2007).

543 39. G. D. Findlay, X. Yi, M. J. Maccoss, W. J. Swanson, Proteomics reveals novel *Drosophila*
544 seminal fluid proteins transferred at mating. *PLoS Biol.* **6**, e178 (2008).

545 40. D. A. Carver, B. A. Ball, Lipase activity in stallion seminal plasma and the effect of lipase
546 on stallion spermatozoa during storage at 5 degrees C. *Theriogenology* **58,** 1587-1595
547 (2002).

548 41. B. Sias *et al*., Cloning and seasonal secretion of the pancreatic lipase-related protein 2
549 present in goat seminal plasma. *Biochim Biophys Acta* **1686,** 169-180 (2005).

550 42. L. Anel-López *et al*., Analysis of seminal plasma from brown bear *(Ursus arctos)* during
551 the breeding season: Its relationship with testosterone levels. *PLoS One* **12,** e0181776
552 (2017).

553 43. F. Vignon, A. Clavert, M. H. Koll-Back, P. Reville, On the glandular origin of seminal
554 plasma lipids in man. *Andrologia* **24,** 341-343 (1992).

555 44. N. S. Juyena, J.Vencato, G. Pasini, I. Vazzana, C. Stelletta, Alpaca semen quality in
556 relation to different diets. *Reprod. Fertil. Dev.* **25,** 683-690 (2013).

557 45. Z. Li *et al*., Lipid droplets control the maternal histone supply of *Drosophila* embryos.
558 *Curr. Biol.* **22,** 2104-2213 (2012).

559 46. J. A. Olzmann, P. Carvalho, Dynamics and functions of lipid droplets. *Nat. Rev. Mol. Cell.*
560 *Biol.* **20,** 137-155 (2019).

561 47. L. K. Sirot, M. F. Wolfner, S. Wigby, Protein-specific manipulation of ejaculate
562 composition in response to female mating status in *Drosophila melanogaster*. *Proc. Natl.*
563 *Acad. Sci. USA* **108,** 9922-992 (2011).

564 48. B. R. Hopkins *et al*., Divergent allocation of sperm and seminal proteome along a
565 competition gradient in *Drosophila melanogaster*. *Proc. Natl. Acad. Sci. USA* **11,** 17925-
566 17933 (2019).

567 49. T. A. Markow, Evolution of *Drosophila* mating systems. *Evol. Biol.* **29,** 73-106 (1996).

568 50. K. R. Ram, M. F. Wolfner, Sustained post-mating response in *Drosophila melanogaster*
569 requires multiple seminal fluid proteins. *PLoS Genet.* **3**, e238 (2007).

570 51. G. D. Findlay, *et al*., Evolutionary rate covariation identifies new members of a protein
571 network required for *Drosophila melanogaster* female post-mating responses. *PLoS Genet.*
572 **10,** e1004108 (2014).

573 52. A. Singh, *et al*., Long-term interaction between Drosophila sperm and sex peptide is
574 mediated by other seminal proteins that bind only transiently to sperm. *Insect Biochem. Mol.*
575 *Biol.* **102**, 43-51 (2018).

576 53. Y. Shiga, M. Tanaka-Matakatsu, S. Hayashi, A nuclear GFP/B-galactosidase fusion protein
577 as a marker for morphogenesis in living *Drosophila*. *Develop. Growth Differ*. **38**, 99-106
578 (1996).

579 54. T. Lee, L. Luo, Mosaic analysis with a repressible cell marker for studies of gene function
580 in neuronal morphogenesis. *Neuron* **22**, 451-461 (1999).

581 55. L. A. Perkins *et al*., The transgenic RNAi project at Harvard Medical School: resources and
582 validation. *Genetics* **201**, 843-852 (2015).

583 56. S. E. McGuire, P. T. Le, A. J. Osborn, K. Matsumoto, R. L. Davis, Spatiotemporal rescue of
584 memory dysfunction in *Drosophila*. *Science* **302**, 1765-1768 (2003).

585 57. S. Hayashi *et al*., GETDB, a database compiling expression patterns and molecular
586 locations of a collection of Gal4 enhancer traps. *Genesis* **34**, 58-61 (2002).

587 58. E. J. Rideout, A. J. Dornan, M. C. Neville, S. Eadie, S. F. Goodwin, Control of sexual
588 differentiation and behaviour by the *doublesex* gene in *Drosophila melanogaster. Nat.*
589 *Neurosci.* **13,** 458-466 (2009).

590 59. V. Greco, M. Hannus, S. Eaton, Argosomes: a potential vehicle for the spread of
591 morphogens through epithelia. *Cell* **106,** 633-645 (2001).

592 60. C. M. Rylett, M. J. Walker, G. J. Howell, A. D. Shirras, R.E. Isaac, Male accessory glands of
593 *Drosophila melanogaster* make a secreted angiotensin I-converting enzyme (ANCE),
594 suggesting a role for the peptide-processing enzyme in seminal fluid. *J. Exp. Biol.* **210**, 3601-
595 3606 (2007).

596 61. R. M. Parton, A. M. Vallés, I. M. Dobbie, I. Davis, Live cell imaging in *Drosophila*

597 *melanogaster*. *Cold Spring Harb. Protoc*. Doi:10.1101/pdb.top75 (2010).

598

599 **Figure legends**

600 **Fig. 1. The accessory gland lumen contains abundant lipophilic microcarriers.**

601 (A, A') Fluorescence image with (A) and without (A') bright-field illumination of paired
602 *Drosophila melanogaster* male accessory glands (AGs) connecting to the ejaculatory duct
603 (ed). Main cells express nuclear GFP under *Acp26Aa*-GAL4 main cell-specific control (green),
604 but secondary cells in distal tip (two of which are marked by yellow arrows in A') do not. (B-
605 E) Confocal sections through AG lumen stained with Nile Red (B, B'; latter is high
606 magnification view), LipidTox (C, C'), LysoTracker Deep Red (D; yellow) and anti-ANCE (red),
607 a soluble secreted protein (E). White arrows mark representative large microcarriers and
608 arrowheads mark small microcarriers. (F) DIC image of lumen from living AG also reveals
609 microcarriers (white arrows). (G) Transmembrane CD8-GFP expressed in main cells marks
610 the apical plasma membrane, but not luminal microcarriers. (H, H') Main cell-expressed
611 GFP-GPI labels microcarriers at their surface (H, H'; white arrowheads) together with the
612 apical surface of the epithelial monolayer (H'; yellow arrows). Nuclei marked with Hoechst
613 (A, A'; blue) or DAPI (B-E, G, H; blue). AG epithelium (ep) (dotted white line in G, H marks
614 approximate basal surface). Scale bars, 10 µm.

615

616 **Fig. 2. SP-GFP is loaded on microcarriers, which disassemble when transferred to females.**

617 (A, B) SP-GFP (green) marks microcarriers in fixed (A) and non-fixed (B) AG lumen, coating
618 the surface of the largest structures (arrows). (C, D) Combined fluorescence and bright-field
619 images of reproductive tract of female mated to a control (C) or SP-GFP (D) male dissected
620 25 min after start of mating (ASM). Anterior (left) and posterior (right) limits of uterus are

demarcated by white asterisks, and seminal receptacle (SR), paired spermathecae (Sp), common oviduct (ov) and mating plug (MP), which autofluoresces in the DAPI channel, are marked. (E, F) Higher magnification views of posterior uterus at this time reveal microcarrier structures have changed (E) with SP-GFP concentrated in microdomains (E'; arrow). (F, G) Later (45 min ASM), many microcarriers have disassembled and some SP-GFP has associated with sperm tails (ST; F, F'), while later still (60 min ASM), few recognisable microcarriers remain and many more strongly labelled sperm tails are observed in the anterior uterus (ST G, G'). Sperm heads (SH) are marked by DAPI. (H, I) Labelled sperm tails (ST) are not present in the seminal receptacles (60-90 min ASM), which contain sperm heads (SH), both in females mated with control (H, H') and SP-GFP males (I, I'). (J, J') Microcarriers remaining in the ejaculatory duct after mating maintain their structure. Outlines of seminal receptacles (H, I) and ejaculatory duct (J, J') are marked by dotted lines. Nuclei marked with DAPI (blue). AG and ejaculatory duct epithelia (ep). Scale bars, 10 µm except C, D, 30 µm.

Fig. 3. SP is essential for proper assembly of microcarriers.

(A, B) Confocal images of LipidTox-labelled microcarriers in lumen of AG from control (A) and $SP^0/Df(SP)$ null (B) males. Mutant male has grossly enlarged microcarriers. (C, D) DIC images of living AGs dissected from control (C, white arrows) and $SP^0/Df(SP)$ (D) males. (E) Microcarrier structural defects in $SP^0/Df(SP)$ null males are rescued by a genomic *SP* construct $SP^0\ SP^+/Df(SP)$. (F, G) Microcarriers enlarge further after multiple matings in $SP^0/Df(SP)$ null (G), but not in wild type (F) males. (H) In $SP^0/Df(SP)$ null males, these enlarged microcarriers are observed when seminal fluid remains in the lumen of the ejaculatory duct after mating. (I, J) Microcarrier size and area profiles for glands shown in A,

B, E. Microcarrier outlines were detected in images of the AG lumen using CellProfiler Software version 2.2.0 (see Methods) and then grouped according to minimum width range (I) or percentage of luminal area occupied by microcarriers in each width range (J). Numbers of microcarriers within each size range are shown above bars (I). *SP^0/Df(SP)* null glands have considerably fewer small microcarriers (<10 µm) and more large microcarriers (>10 µm) than the other genotypes. The enlarged microcarriers in *SP^0/Df(SP)* null glands contain most of the lipid in the AG lumen, as estimated by LipidTox staining area. Nuclei marked with DAPI (blue). AG (A-G) or ejaculatory duct (H) epithelium (ep). Scale bars, 10 µm.

Fig. 4. Knockdown of *SP* in main cells also produces highly enlarged microcarriers.

All specimens are stained with LipidTox. (A) Confocal image of microcarriers in lumen of AG from control male. (B-C) Knockdown of *SP* in main cells at 29°C with two RNAis, *UAS-SP-RNAi#1* (B; IR2 from (11)) and *UAS-SP-RNAi#2* (C; TRiP.JF02022) produces enlarged microcarriers. (D-F) Multiple mating of *SP* knockdown males leads to further increases in microcarrier size (E, F), presumably via fusion, which is not observed in controls (D). (G) *SPR* mutant males (homozygous *Df(1)Exel6234*) have normal microcarriers. (H-K) The *SP^0/Df(SP)* null phenotype (H) is rescued by a wild type *SP* genomic construct in *SP^0 SP^+/Df(SP)* males (I), but not by genomic constructs expressing mutant $SP^{\Delta 2\text{-}7}$ (J) or SP^{QQ} (K). Nuclei marked with DAPI (blue). AG epithelium (ep). Scale bar in (A), 10 µm applies to all panels.

Fig. 5. Microcarriers from *SP* null males do not dissipate normally when transferred to females during mating.

(A, B) A genomic SP-GFP fusion construct labels *SP* wild-type microcarriers (A), and enlarged defective microcarriers in the AG of $SP^0/Df(SP)$ null males, though it does not rescue the associated microcarrier phenotype (B). (C-F) Combined fluorescence and bright-field images at 25-30 min ASM of whole reproductive tracts (anterior on left; C, D) and posterior uterus at higher magnification (E, F) from females mated either with control males expressing SP-GFP (C, E) or with $SP^0/Df(SP)$ null males expressing SP-GFP (D, F). Microcarrier-like structures from the $SP^0/Df(SP)$ null male are fused together in a globular mass, whereas microcarriers from control males do not fuse, but carry localised SP-GFP puncta. (G, H) At 45-50 min ASM, SP-GFP-positive material remains in a globular mass in females mated with $SP^0/Df(SP)$ null males, which extends into the anterior uterus, unlike controls (H, H'). This mass contains a few intensely labelled sperm tails (arrows). By contrast, SP-GFP from wild type males has dispersed, although some intense fluorescent puncta remain (G, G'), and often many sperm tails in the anterior uterus are labelled (arrows in G'). (I) Schematic representing microcarrier structure in accessory glands of wild-type and $SP^0/Df(SP)$ null males, as visualised using the SP-GFP fusion protein, and the changes that take place 25-30 min ASM in the female reproductive tract. In (C, D), anterior (left) and posterior (right) boundaries of uterus are demarcated by asterisks and seminal receptacle (SR), one of the two spermathecae (Sp), oviduct (ov) and mating plug (MP) are labelled. Nuclei marked with DAPI (blue). AG epithelium (ep), uterine epithelium (Uep). Scale bars, 10 µm except for C, D, 30 µm.

Fig. 6. Co-evolution of microcarrier morphology and SP in *Drosophila* species.

(A) Phylogenetic tree of *Drosophila* species used in this study. All species except *D. mojavensis* have a putative SP homologue. Adapted from http://flybase.org/blast/. (B-K) LipidTox staining of AGs from 6-day-old virgin males from selected *Drosophila* species, namely *D. melanogaster* (B), *D. simulans* (C), *D. sechellia* (D), *D. erecta* (E), *D. yakuba* (F), *D. pseudoobscura* (G), *D. persimilis* (*H*), *D. willistoni* (*I*), *D. virilis* (*J*) and *D. mojavensis* (K). For (I-K), where LipidTox microcarriers are not readily detectable, bright-field images of the same glands are shown (I'-K'), as well as DIC images (I''-K'') of different glands. Insets in (I, J, K) are images of AG with epithelial layer punctured to fully expose luminal contents to LipidTox stain, revealing stained structures only in *D. willistoni*. Note that different subgroups have noticeably different microcarrier size, shape and density. Nuclei marked with DAPI (blue). AG epithelium (ep). All scale bars, 10 µm; scale bar in (B) applies to (B-H); in (I), applies to (I-K) and (I'-K'); and in (I'') applies to (I''-K'').

Supplementary Figures.

Fig. S1. Structure and cargos of accessory gland microcarriers.

(A, B) Both main cell-expressed transmembrane CD8-RFP (A) and the lipid bilayer dye PKH26 (B) mark the main cell apical membrane (A', B'), but not the luminal microcarriers labelled by SP-GFP (merge in A, B). (C) Secreted GFP is not preferentially partitioned on to microcarriers. (D) In the AG lumen, secreted secondary cell-expressed GFP-GPI is primarily associated with puncta (arrowheads; cell boundaries seen in bright-field image; D') and does not appear to be loaded on to microcarriers. (E) Transmission electron micrograph of AG lumen showing a range of sizes of microcarriers (arrowheads) (F-H). The N-terminus of mature SP with a C-terminal GFP tag (F; SPn-GFP), full length SP with a central GFP tag (G; SPn-GFP-SPc) and the C-terminus of SP with an N-terminal GFP tag (H; GFP-SPc) all concentrate on microcarriers when expressed in main cells albeit at lower levels for SPn-GFP. (I) Size distribution of microcarriers in LipidTox-stained AG lumen from image in Fig. 1B'. Nuclei marked with DAPI (blue). AG epithelium (ep). Scale bars, 10 µm.

Fig. S2. Loss or reduction of SP disrupts microcarrier morphology.

(A-D) LipidTox-stained microcarriers are highly enlarged in SP^0/SP^0 homozygous males (B) when compared to controls (A). Expressing a third RNAi targeting *SP* transcripts *(UAS-SP-RNAi#3*; v109175) induces the formation of enlarged microcarriers (D), unlike controls (C). Nuclei marked with DAPI (blue). AG epithelium (ep). Scale bars, 10 µm.

Fig. S3. *SP* mutant, *SP* RNAi and some *SP* rescue glands have enlarged microcarriers.

(A-C) Histograms showing percentage of microcarrier area within given microcarrier minimum width ranges. (A) More lipid is incorporated into microcarriers in larger size ranges in homozygous SP^0/SP^0 gland (from Fig. S2B) than in control glands (Fig. S2A). (B) *SP*-RNAi knockdown in main cells increases the incorporation of lipid into larger microcarriers (from glands shown in Fig. 4B, C) compared with control glands (Fig. 4A). (C) Expression of $SP^{\Delta 2\text{-}7}$ or SP^{QQ} (from glands shown in Fig. 4J, K) fails to rescue the $SP^0/Df(SP)$ null phenotype (Fig 4H) when compared with $SP^0\ SP^+/Df(SP)$ rescue (Fig. 4I). Main cell (MC).

Fig. S4. Rapid evolution of SP sequences correlates with changes in microcarrier morphology, size and abundance in diverse *Drosophila* species.

SP protein sequence alignment for the different *Drosophila* species used in this study. Species are clustered according to subgroup. Conserved amino acids are highlighted or underlined; blue = conserved across all SP-expressing species; green = conserved in *melanogaster* and *obscura* groups; pink = conserved in *melanogaster* group; grey, brown or yellow = conserved within a single species cluster. The subdivision of these groups correlates with SP protein sequence, and shape, size and abundance of microcarriers in each species. Adapted from (24).

SI Movie 1. Live imaging of SP-GFP-labelled microcarriers.

746 *Z* stack through distal tip of live SP-GFP AG. Lysotracker-Red (red; used at high

747 concentrations) marks epithelial layer of gland. Confocal sections were captured at 1.5 µm

748 intervals on *Z* axis.

749

750

751

752

753 **Fig. 1**

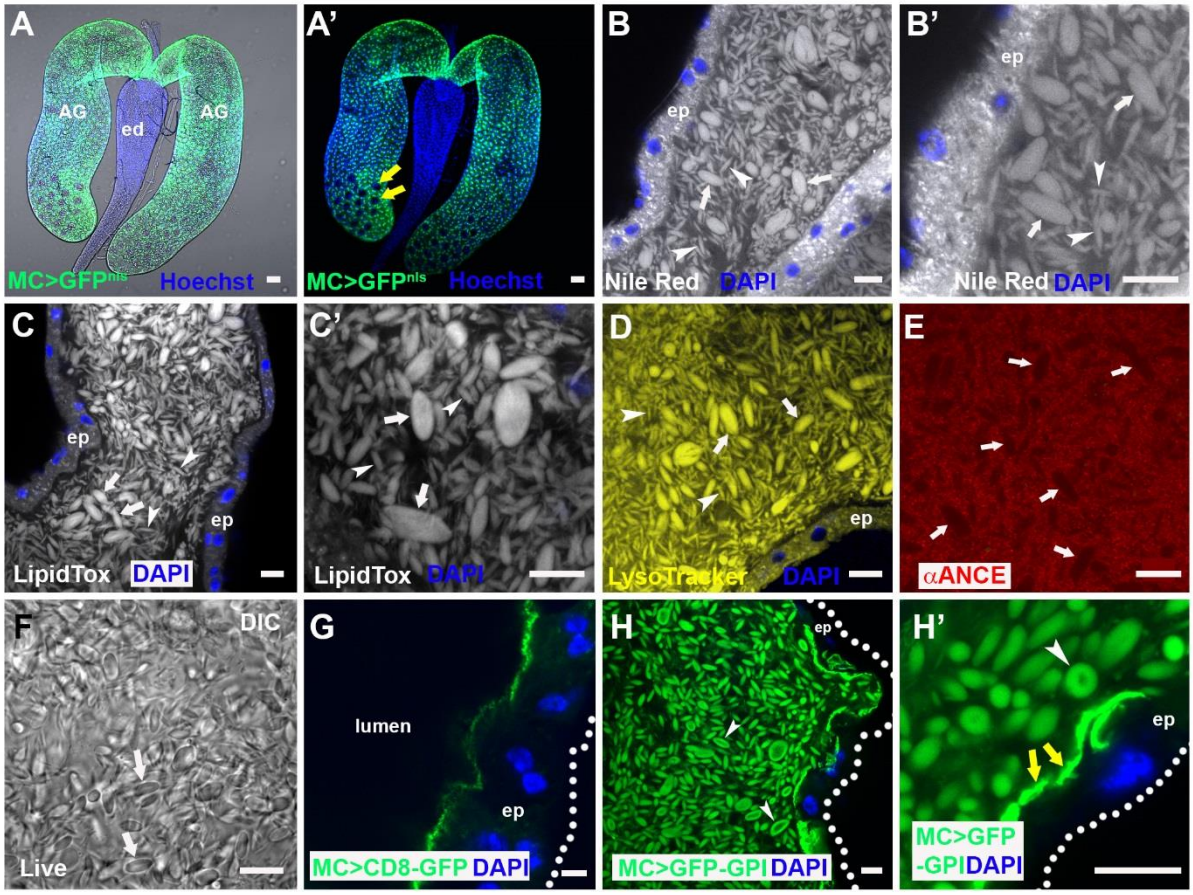

754

755

Fig. 2

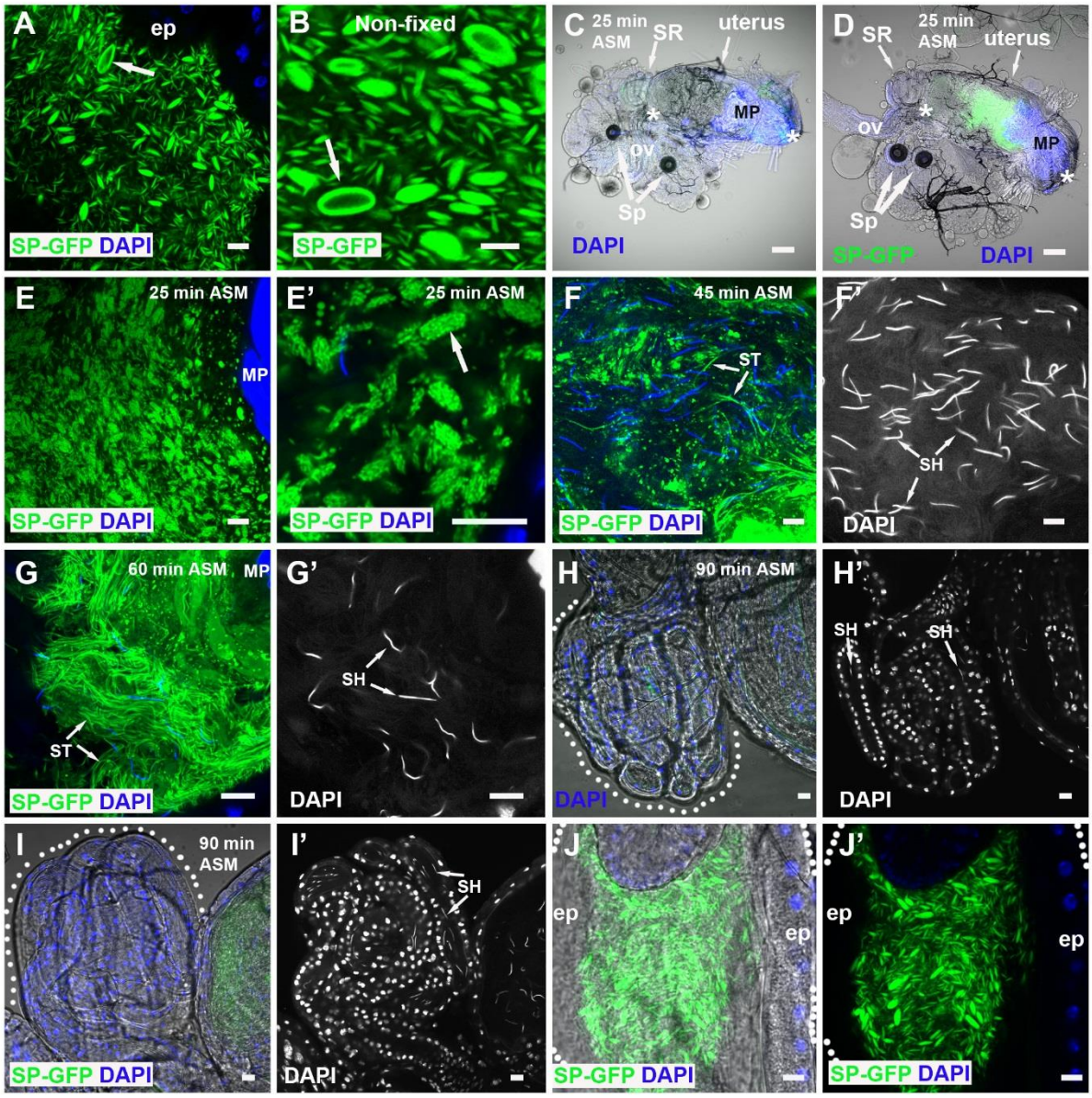

760 **Fig. 3**

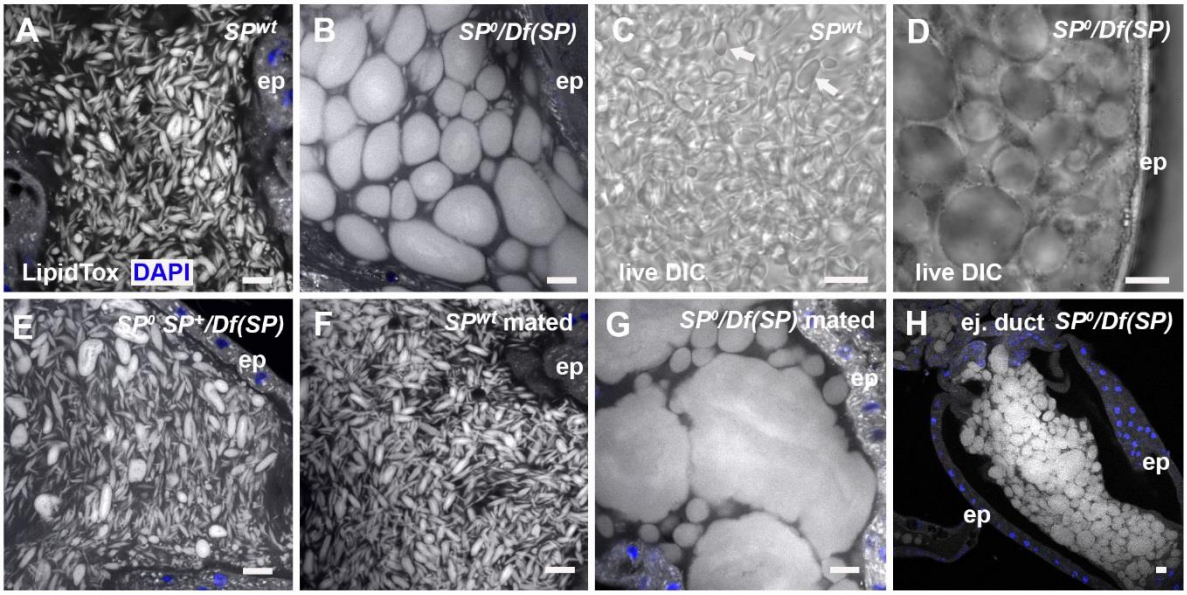

I

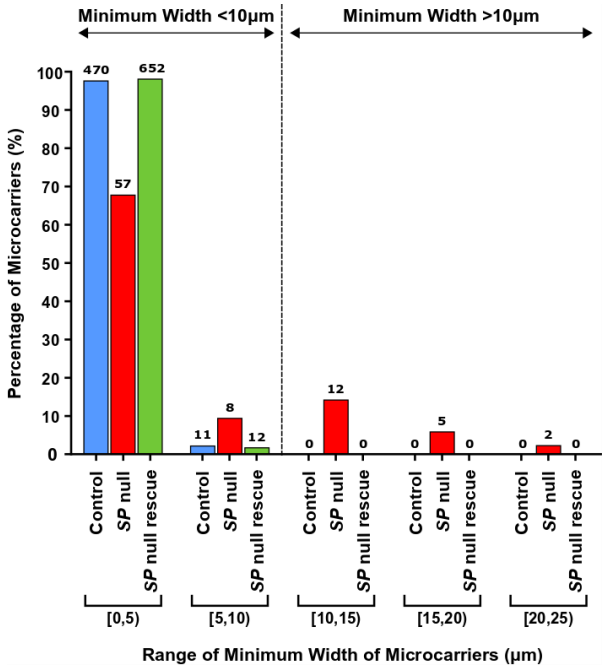

J

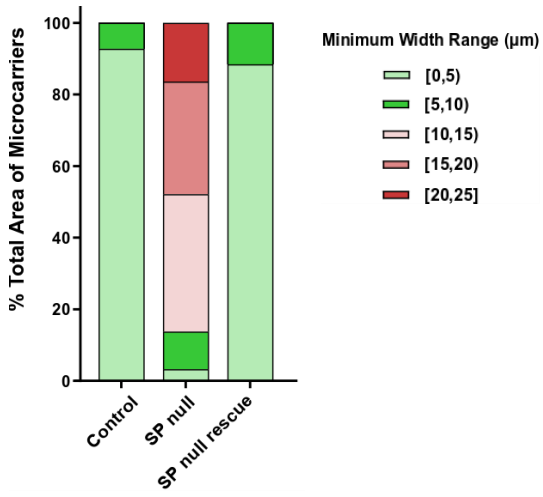

761

762

Fig. 4

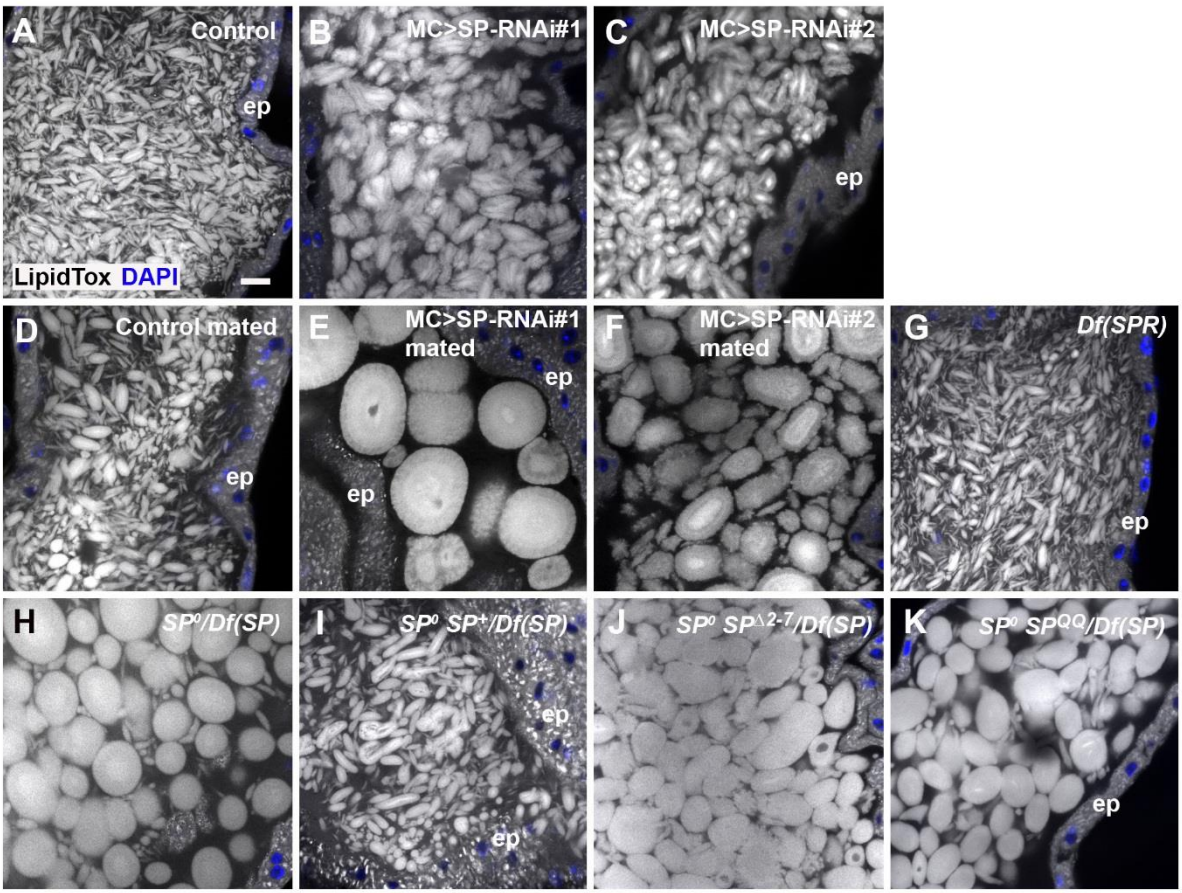

766 **Fig. 5**

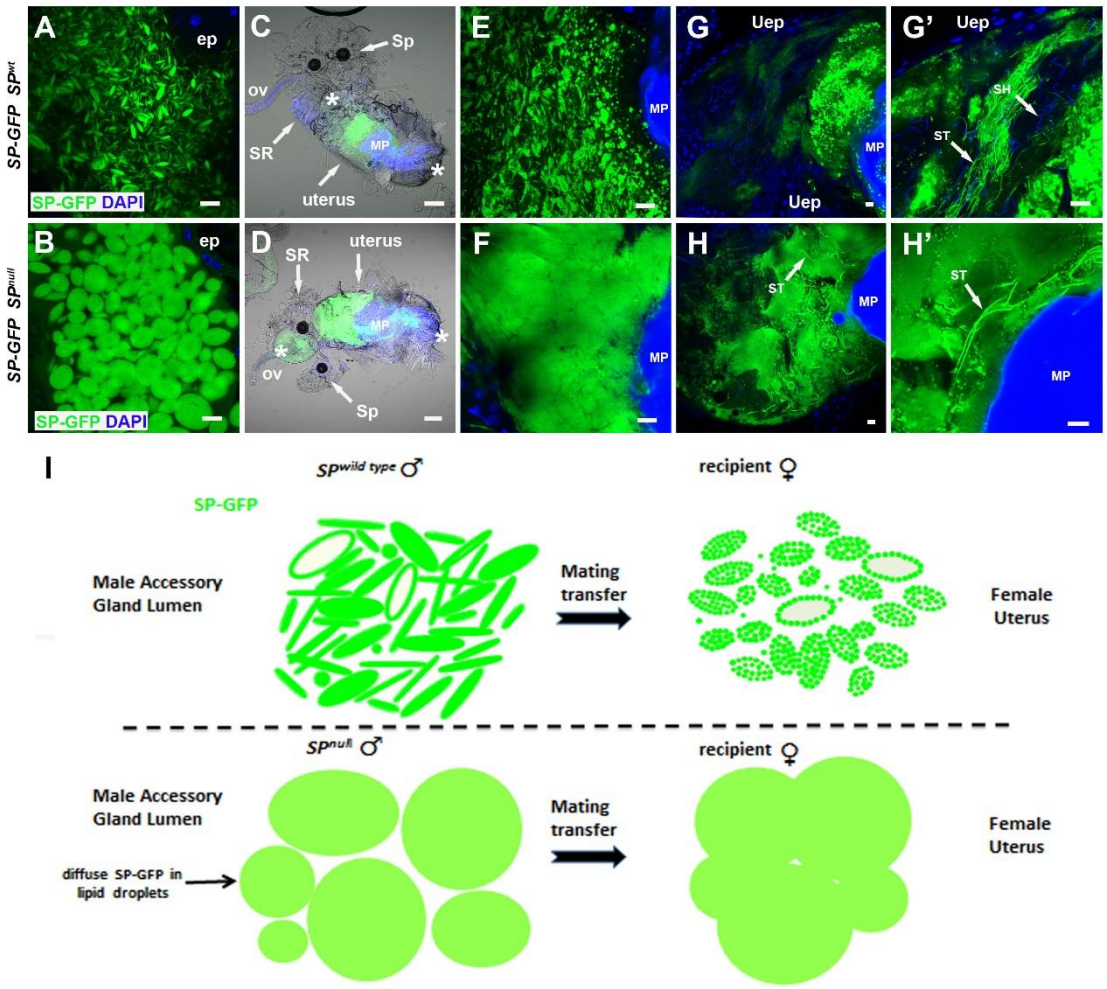

767

768

769

770

771 **Fig. 6**

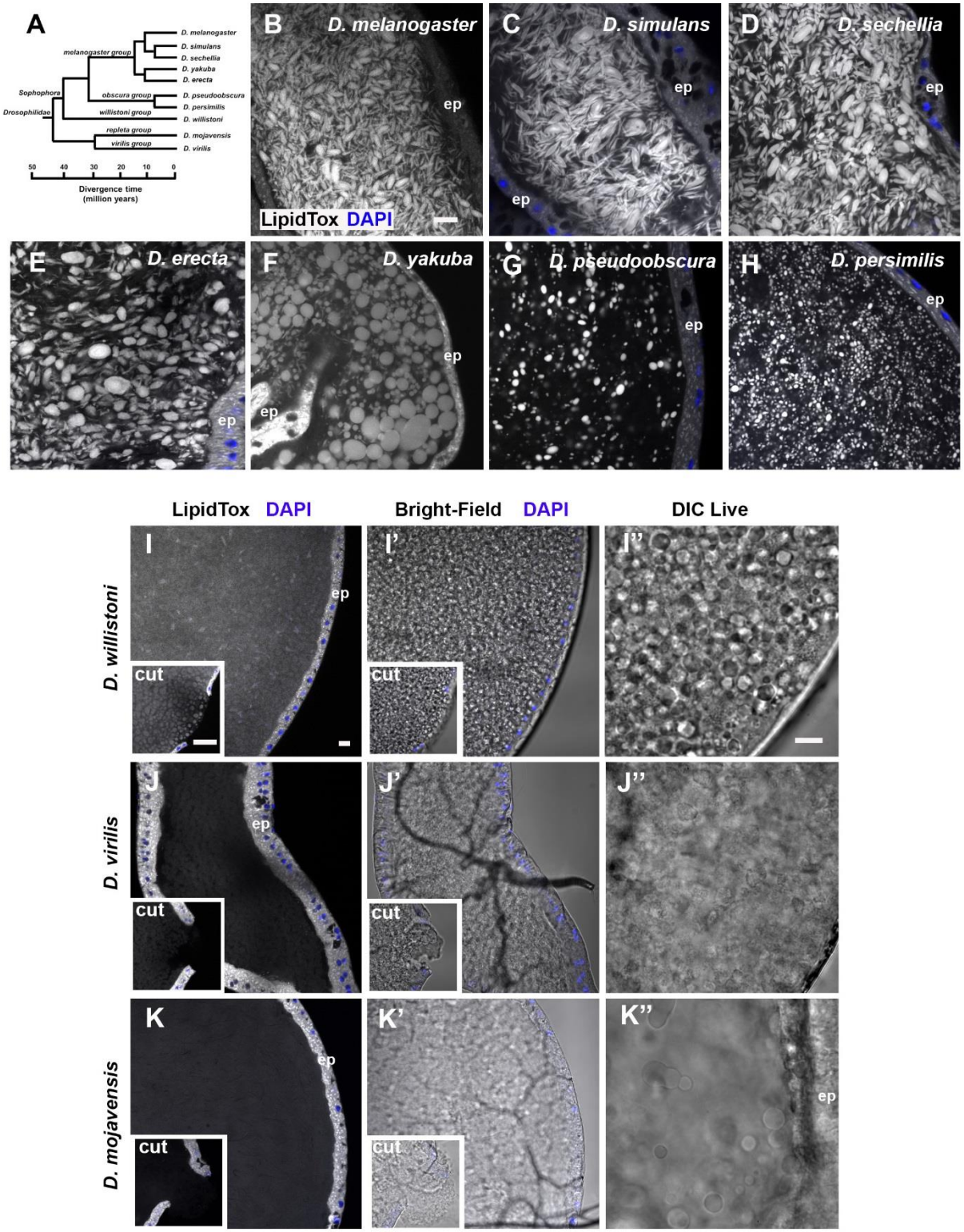

772

773

774 **Fig. S1**

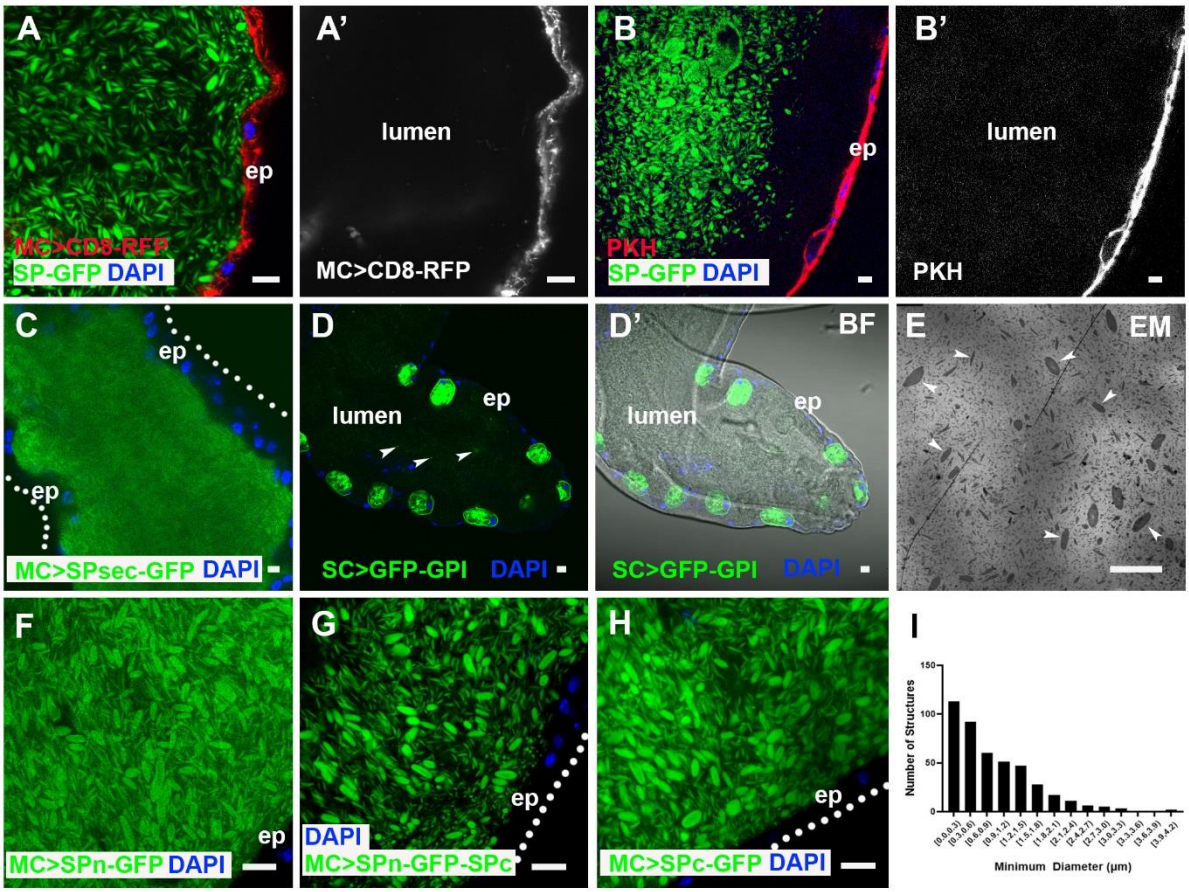

775

776

777 **Fig. S2**

778

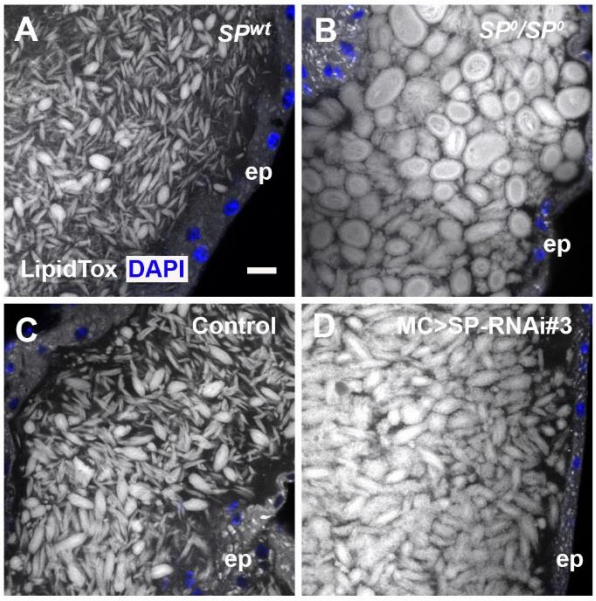

779

780 **Fig. S3**

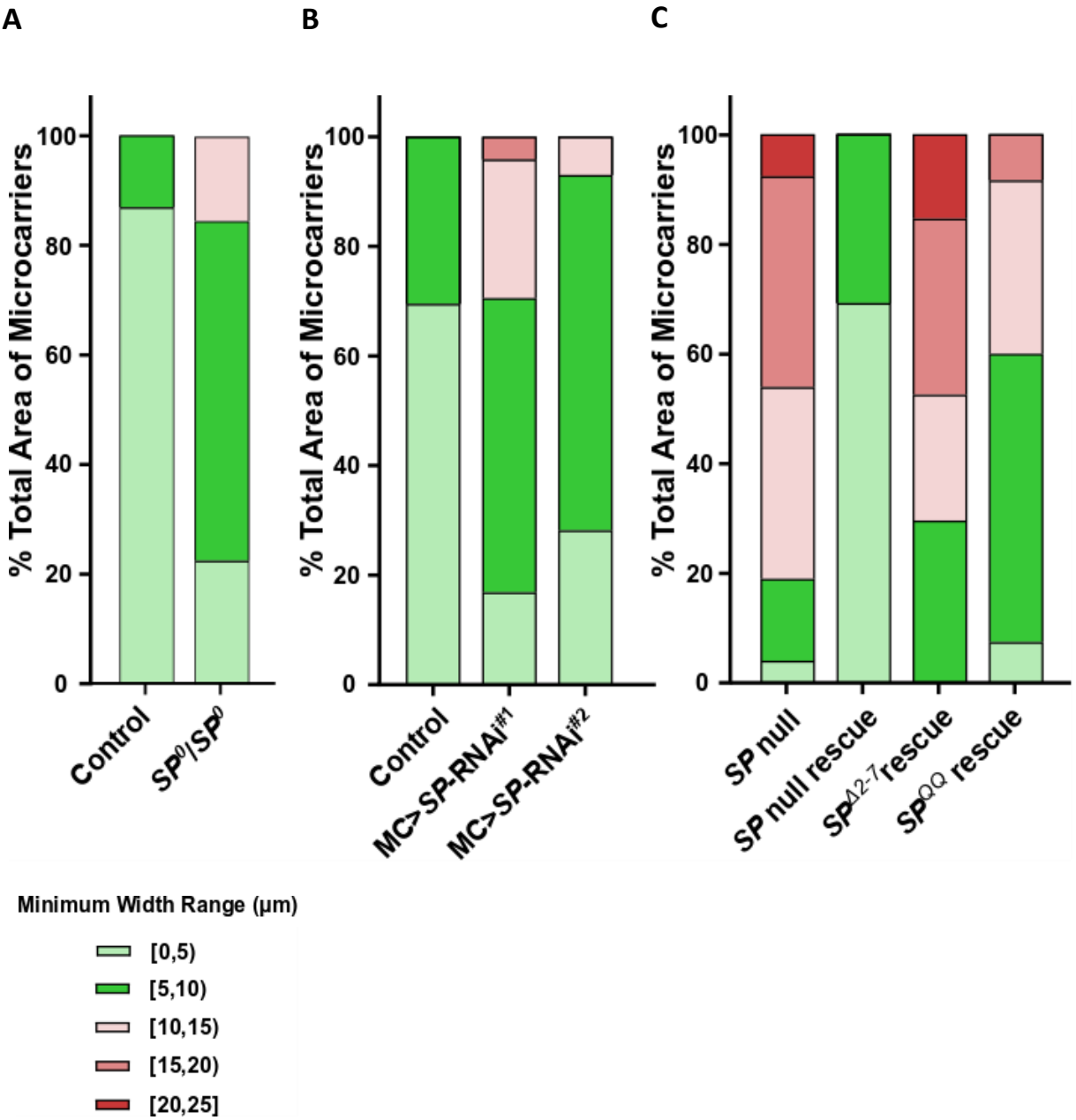

785

786

787

788

Fig. S4

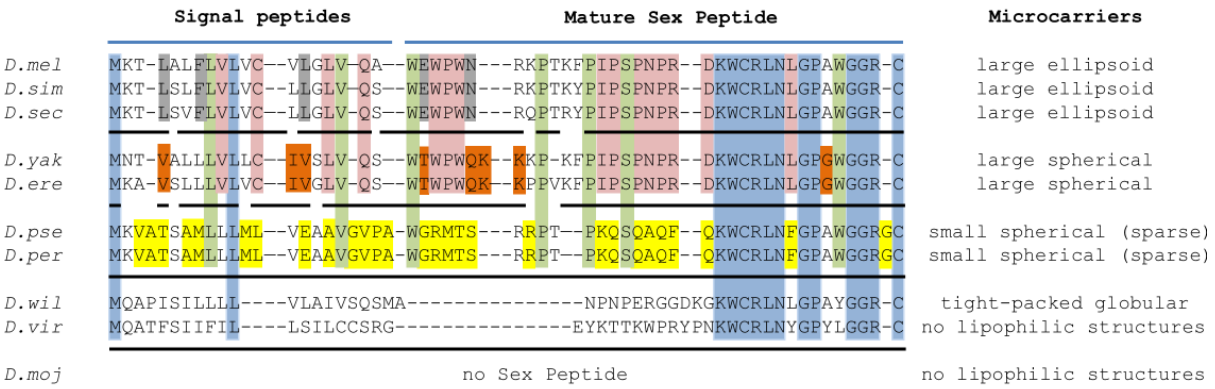

800 **Supporting information Movie 1.**

801 **Live imaging: *Z* stack through distal tip of SP-GFP AG.**

802

803